



UNIVERSITÉ DE NANTES - IMT ATLANTIQUE

CEA PARIS-SACLAY

Mathieu Ronayette

Measurement of the exclusive ϕ photoproduction on a proton with the CLAS12 experiment at Jefferson Lab

Rapport de stage M2
01/03/2025 - 31/07/2025

Supervisor:
Pierre Chatagnon

Contents

1	Introduction	1
2	Physics motivations	2
2.1	Quantum Chromodynamics	2
2.2	Parton Distribution Functions (PDFs)	3
2.3	Electro-magnetic Form Factors (FFs)	4
2.4	Generalized Parton Distributions (GPDs)	4
2.5	The ϕ production mechanism	5
3	Experimental setup	6
3.1	Jefferson Lab overview	6
3.2	The Continuous Electron Beam Accelerator Facility (CEBAF)	6
3.3	The CLAS12 detector	6
3.3.1	CLAS12 general design	6
3.3.2	The target	8
3.3.3	CLAS12 Central Detector (CD)	8
3.3.4	CLAS12 Forward Detector (FD)	8
4	Measurement of the cross section of the photoproduction of ϕ with CLAS12	10
4.1	ϕ quasi-real photoproduction	10
4.2	Particle identification	11
4.2.1	Proton identification	11
4.2.2	Electron and positron identification	13
4.3	Events selection	14
4.4	Experimental cross section	15
4.5	Extraction of the ϕ meson yield	16
4.6	Acceptance estimation	18
4.6.1	Generator of ϕ events	18
4.6.2	Acceptance estimation	20
4.7	Luminosity of the RGA dataset	21
4.8	Photon flux calculation	21
4.9	Results on cross section and differential cross section	23
5	Conclusion and outlook	25

1 Introduction

The visible matter of the universe is mostly made of atoms. Since the beginning of the 20th century and Rutherford’s alpha particle scattering experiment, it is known that atoms are mostly empty space and that their mass is concentrated in a central nucleus. Rutherford’s experiments in 1919 and Chadwick’s in 1932 established that the atomic nucleus is composed of protons and neutrons, opening a new line of research into the structure of nucleons. In 1969, the SLAC collaboration, through deep inelastic scattering experiments, demonstrated that nucleons themselves are composed of even smaller particles—quarks and gluons. The parton model, which describes the particles making up nucleons, was developed subsequently. These experiments and discoveries laid the foundation of hadronic physics and have contributed to a better understanding of the interactions between the fundamental constituents of visible matter in the universe.

Quantum Chromodynamics (QCD), which describes the interactions between quarks via the exchange of gluons, is calculable at high energy. Indeed, its coupling constant decreases as the energy increases, which allows for a perturbative approach at high energy. However, at low energy, this perturbative approach is no longer valid. It is therefore necessary to introduce new objects, Structure Functions, to describe the dynamics of partons inside hadrons.

To achieve this, structure functions such as Form Factors (FFs) and Parton Distribution Functions (PDFs) are used to describe, respectively, the transverse position of partons in the nucleon and their fraction of longitudinal momentum. FFs allow the determination of the nucleon’s radius, while PDFs encode the momentum distributions of the partons. The generalization of FFs and PDFs into Generalized Parton Distributions (GPDs) makes it possible to obtain more fundamental information about nucleons, such as spin decomposition and pressure distribution inside the nucleon.

The information obtained from GPDs helps shed light on unresolved properties of nucleons. It is currently difficult to explain how the elementary constituents of the proton contribute to its total spin of $1/2$. Similarly, the contribution of the elementary constituents to the proton’s mass is still not well understood.

Extracting the cross-section of exclusive processes allows one to access the GPDs of partons. The aim of this internship is to extract the cross-section of the photo-production of the ϕ meson (composed of a strange and an anti-strange quarks) in the e^+e^- channel ($\gamma p \rightarrow e^+e^- p$). This involves studying the interaction between a real photon emitted by an electron from a 12 GeV accelerated beam and a proton. Extracting this cross-section allows to access the gluon GPDs and explore the gluon dynamics within the proton. Data collected by the CLAS12 experiment, a large-acceptance detector in Hall B of Jefferson Lab (Virginia, USA), specifically designed for hadronic physics measurements, will be analyzed.

2 Physics motivations

2.1 Quantum Chromodynamics

Quantum Chromodynamics (QCD) is the theory describing the interactions between particles carrying color charges (red, green, and blue), such as quarks, which interact via the exchange of massless mesonic particles (gluons). The gluons, which also carry color charges, can also interact with each other. The theory of QCD is described by a Lagrangian invariant under the $SU(3)$ symmetry. Its Lagrangian is written as:

$$\mathcal{L} = -\frac{1}{4}F_{uv}^a F^{auv} + \sum_k \bar{\psi}_{ki}(i\cancel{D}_{ij} + m_k)\psi_{kj}, \quad (1)$$

where ψ_k represents the quark field and k runs over the quark flavors, while i and j run over the colors. F_{uv}^a is the gluon field strength tensor and is written as:

$$F_{uv}^a = \partial_u A_v^a - \partial_v A_u^a + g f^{abc} A_u^b A_v^c, \quad (2)$$

where A_u^a is the gluon field and a runs over the 8 kinds of gluons. The gauge derivative \cancel{D}_{ij} is written as:

$$\cancel{D}_{ij} = \partial_u \delta_{ij} - ig A_u^a T_{ij}^a, \quad (3)$$

where T_{ij}^a are the 8 $SU(3)$ generator matrices. f^{abc} are the $SU(3)$ structure constants and g is the QCD coupling constant. The strong fine-structure constant α_s is defined as:

$$\alpha_s = \frac{g^2}{4\pi}. \quad (4)$$

The $SU(3)$ structure of the Lagrangian gives rise to the two main properties of QCD: asymptotic freedom and confinement. Confinement refers to the fact that quarks and gluons are never observed as free particles. They are always observed in bound states. This is due to the fact that the only stable QCD states are color-neutral. Thus, when the distance between two quarks increases, the potential energy increases until it becomes sufficient to produce a quark-antiquark pair, thereby restoring the net color neutrality of the system.

The second property, asymptotic freedom, stems from the fact that the value of α_s depends on the renormalization scale μ as:

$$\alpha_s = \frac{12\pi}{(33 - 12n_f) \ln(\frac{\mu^2}{\Lambda^2})}, \quad (5)$$

where n_f is the number of flavors and $\Lambda = 250$ MeV. We thus see that the constant α_s decreases as the energy scale increases [1]. At high energies, QCD calculations can therefore be done using a perturbative approach, as powers of α_s become negligible. On the other hand, at low energies, the perturbative approach is no longer valid, and other tools are needed to describe quark and gluon interactions. To better understand the internal structure of nucleons, one must use structure functions (see section 2.2 and 2.4).

2.2 Parton Distribution Functions (PDFs)

Hadrons such as protons and neutrons are not elementary particles, but systems composed of quarks and gluons, collectively called partons. When a proton is involved in a high-energy collision, it is one of its constituent partons that actually interacts. The statistical properties of these partons inside the proton are described by parton distribution functions (PDFs).

The PDFs, usually denoted $f_i(x, Q^2)$, give the probability of finding a parton of type i (up quark, down quark, gluon, etc.) in the proton, carrying a fraction x of the longitudinal momentum of the proton, at a given energy scale Q^2 .

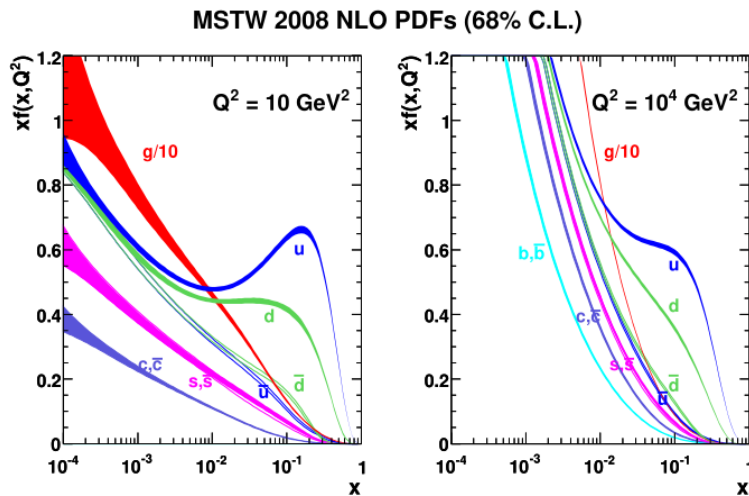


Figure 1: Proton PDFs $xf(x, Q^2)$ as a function of x , where x represents the fraction of longitudinal momentum carried by the parton and $f(x, Q^2)$ represents the associated probability density. The PDFs are plotted for different partons: $u, d, s, \bar{u}, \bar{d}, \bar{s}$ and gluons. The left plot is at the scale $Q^2 = 10 \text{ GeV}^2$ and the right one at $Q^2 = 10^4 \text{ GeV}^2$. Figure from [2].

Parton distribution functions (PDFs) allow the prediction of particle production cross sections in collisions involving hadrons, such as protons. Thanks to the QCD factorization high-energy theorem, it is possible to separate contributions associated with two distinct scales: a hard scale, related to the elementary interaction between partons (calculable perturbatively), and a soft scale, related to the internal structure of the proton, modeled by PDFs and extracted from experimental data. For example, the total cross section of a process in a proton-proton collision is written as:

$$\sigma = \sum_{i,j} \int_0^1 dx_1 \int_0^1 dx_2 f_i(x_1, Q^2) f_j(x_2, Q^2) \hat{\sigma}_{ij}(x_1, x_2, Q^2), \quad (6)$$

where $f_i(x_1, Q^2)$ and $f_j(x_2, Q^2)$ are the PDFs of partons from each proton, and $\hat{\sigma}_{ij}$ is the cross section of the interaction between partons i and j .

2.3 Electro-magnetic Form Factors (FFs)

Electro-magnetic Form Factors (FFs) are structure functions that describe the internal structure of a hadron (such as the proton or neutron) when probed via an electromagnetic interaction, through the exchange of a virtual photon.

For example, in elastic scattering $e^- p \rightarrow e^- p$, the interaction proceeds via the exchange of a virtual photon, and the amplitude depends on two electromagnetic form factors of the proton: the electric form factor $G_E(Q^2)$ and the magnetic form factor $G_M(Q^2)$, both of which are functions of the virtuality Q^2 of the exchanged photon. In certain approximations (notably at low Q^2), one can interpret their Fourier transform as a spatial charge density:

$$\rho(\vec{r}) = \int \frac{d^3\vec{q}}{(2\pi)^3} e^{i\vec{q}\cdot\vec{r}} G_E(Q^2). \quad (7)$$

Thus, the FFs provide insight into the spatial distribution of charge inside the proton.

2.4 Generalized Parton Distributions (GPDs)

Generalized Parton Distributions (GPDs) was developed in the early 90's [3] [4] and extend the concept of PDFs and FFs by incorporating information both on the momentum fraction carried by the partons and on their transverse spatial position within the proton. They are involved in the description of exclusive processes such as Deeply Virtual Compton Scattering (DVCS) [5](diagram presented in Figure 2) or exclusive meson photoproduction (presented in section 2.5).

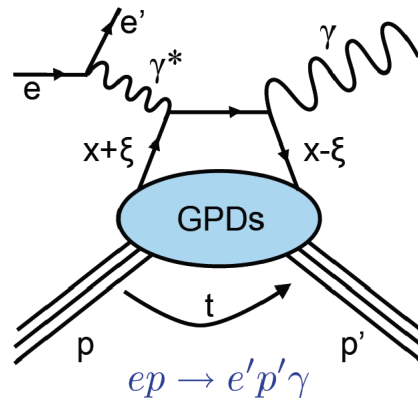


Figure 2: Diagram representing Deeply Virtual Compton Scattering (DVCS).

There are four unpolarized GPDs : $H(x, \xi, t)$, $E(x, \xi, t)$, $\tilde{H}(x, \xi, t)$ and $\tilde{E}(x, \xi, t)$. These GPDs depend on three variables: x , the longitudinal momentum fraction carried by the parton; ξ , related to the asymmetry between the incoming and outgoing struck parton momenta; and the Mandelstam variable $t = (p' - p)$, the squared momentum transfer between protons (sensitive to transverse structure). Finally, GPDs

also depend on the energy scale Q^2 of the process.

The GPDs generalize both the PDFs (in the limit $\xi = 0$ and $t = 0$) and the electromagnetic form factors (when integrating over x). GPDs provide access to a 3D imaging of the proton (one longitudinal momentum dimension and two transverse spatial dimensions). They are therefore a key tool in probing the structure of the proton, particularly in experimental programs such as those carried out at Jefferson Lab.

2.5 The ϕ production mechanism

This section describes the photoproduction mechanism of the ϕ meson and its connection to the gluons distribution inside the proton.

Figure 3 illustrates the photoproduction mechanism of vector mesons (for example : ω , ϕ , J/ψ , and Υ). The photon fluctuates into a quark-antiquark pair $q\bar{q}$ which interacts with the gluons in the proton. In the case of the ϕ meson, an strange and a anti-strange quark are produced. Since the mass of the ϕ is 1.019 GeV and the proton is at rest, in fix-target kinematics, the photon must have a minimum energy of 1.57 GeV to produce a ϕ meson.

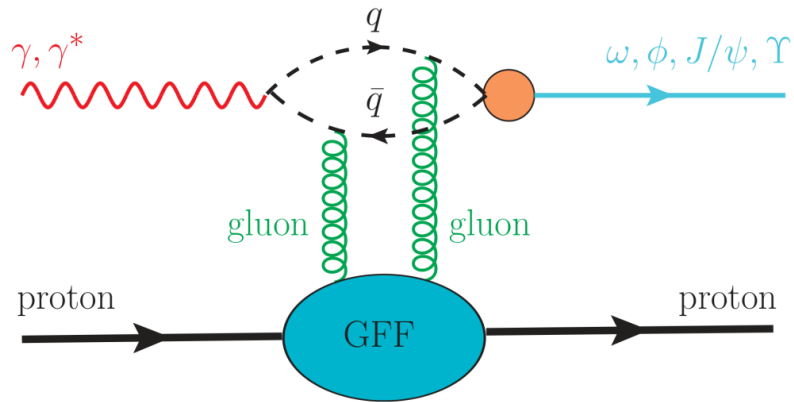


Figure 3: Diagram representing the ϕ production mechanism. There are a photon and a proton in the initial state. There are a recoil proton and a meson in the final state. Figure from [6].

Since the contribution of sea quark-antiquark pairs inside the proton is negligible, gluons play a major role in the creation of the $s\bar{s}$ pair. Extracting the photoproduction cross section of the ϕ thus makes it possible to access the gluon GPDs.

3 Experimental setup

This section describes the experimental program conducted at the Thomas Jefferson National Accelerator Facility. An overview of the laboratory will be presented, followed by a presentation of the electron accelerator and the CLAS12 detector.

3.1 Jefferson Lab overview

The Thomas Jefferson National Accelerator Facility (JLab) is a laboratory of the U.S. Department of Energy, located in Newport News, Virginia (USA). The experiments conducted at this laboratory bring together more than 2,000 scientists from around the world. Since its establishment in 1984, it has been dedicated to the study of the strong interaction.

Jefferson Lab consists of an electron accelerator that produces a continuous electron beam of up to 12 GeV. The electrons are then directed into four different experimental Halls. Each Hall is dedicated to a different physics program and is equipped with its own detector. The CLAS12 detector (CEBAF Large Acceptance Spectrometer 12) is located in Hall B.

3.2 The Continuous Electron Beam Accelerator Facility (CE-BAF)

The main facility at Jefferson Lab is CEBAF, a superconducting radio-frequency accelerator. It delivers an electron beam reaching up to 12 GeV for Hall D and 11 GeV for Halls A, B, and C. The electrons are generated at the injector from a gallium arsenide photocathode, illuminated by four circularly polarized lasers (one for each hall). The polarization allows the extraction of polarized electrons. The lasers operate at 250 MHz and are individually phase-shifted to distinguish each electron bunch. The power of each laser can be individually controlled, allowing the beam current to be adjusted independently for each hall.

The beam is then injected into the accelerator, which consists of two linacs with 25 cryomodules each. The linacs are connected by recirculation arcs, and a different arc is used at each pass of the beam (as seen in figure 4). The maximum energy of about 11 GeV for Halls A, B, and C is reached after five passes. Two separators (750 MHz and 500 MHz) then split the beam between the halls. During the data-taking period in Hall B, the maximum energy reached was 10.6 GeV with a luminosity of $10^{35} \text{ cm}^{-2}\text{s}^{-1}$ [7].

3.3 The CLAS12 detector

3.3.1 CLAS12 general design

The CLAS12 detector is installed in Hall B [8]. It features a very large angular acceptance, allowing the measurement of both inclusive and exclusive processes over

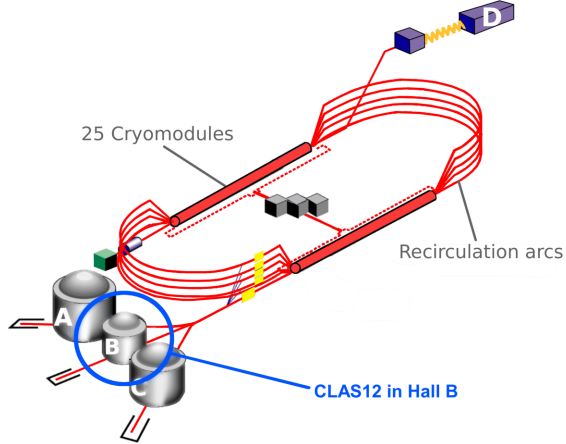


Figure 4: Schematic description of the continuous electron beam accelerator facility (CEBAF).

a broad phase space.

CLAS12 is composed of two main sub-detectors: the Central Detector (CD) and the Forward Detector (FD). The FD detects particles with polar angles between 5° and 35° relative to the beam direction. The CD measures recoil particles emitted backward with polar angles between 35° and 135° . In addition to the CD and FD, the Forward Tagger (FT) covers very small polar angles. It is dedicated to tagged photoproduction measurements and is located close to the beamline downstream of the target. Finally, a solenoid magnet and a toroidal magnet are used to bend the trajectory of charged particle and measure their momentum in the CD and FD, respectively. Figure 5 shows an overview of the detector.

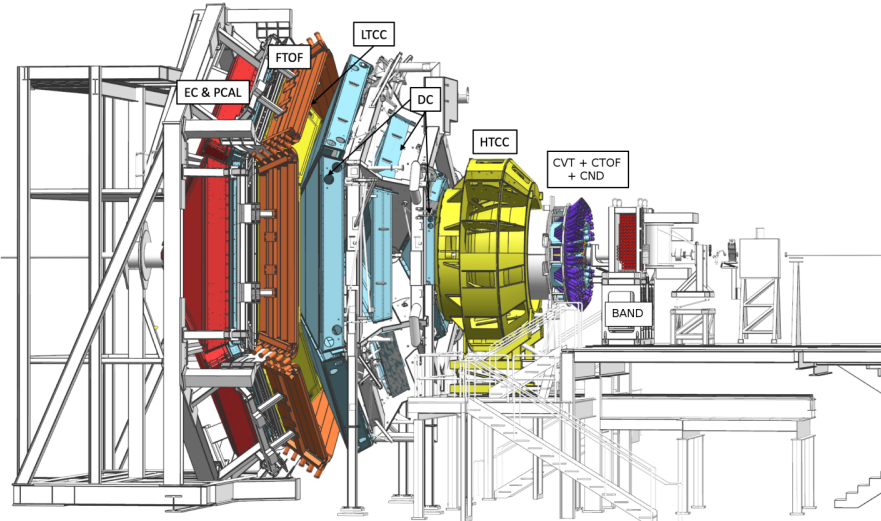


Figure 5: Overview of the CLAS12 detector in Hall B. Figure from [8].

3.3.2 The target

The experiments conducted with CLAS12 are grouped into "run groups" (RGs). Experiments within the same run group use the same experimental setup and the same target. The first two run groups of CLAS12 were performed with unpolarized targets.

The cryogenic target consists of a 5 cm Kapton cone containing the target material. The first run group (RG-A) used liquid hydrogen (LH_2).

The beam enters and exits the target through 30 μm thick aluminum windows. The beam position at the target is monitored using a Beam Offset Monitor (BOM). This system uses a glass cylinder placed parallel to the beam. The Cherenkov light produced by the beam halo is collected via optical fibers and read out with a multi-anode photomultiplier tube (PMT), allowing the beam offset at the target position to be determined [9].

3.3.3 CLAS12 Central Detector (CD)

The Central Detector (CD) of CLAS12 is located between the target and the inner wall of the solenoid magnet. It is a barrel detector with 2π azimuthal coverage. It is composed of a tracking system, the Central Vertex Tracker (CVT). The CVT itself consists of two sub-systems: a Silicon Vertex Tracker (SVT) in the innermost region, surrounded by a Micromegas Vertex Tracker (MVT). The CVT is used to measure the momentum of charged particles by analyzing the curvature of their helical trajectories in the magnetic field produced by the solenoid. The momentum p perpendicular to the magnetic field B is given by:

$$R = \frac{p}{qB}, \quad (8)$$

where R is the radius of curvature and q is the charge of the particle. In practice, only the ratio $\frac{p}{q}$ is obtained from the track radius. The sign of the charge q is determined by the curvature direction of the trajectory, as particles with opposite charges bend in opposite directions in a magnetic field.

The Central Detector also includes two time-of-flight detectors: the Central Time Of Flight (CTOF) and the Central Neutron Detector (CND), used for the identification of charged and neutral particles, respectively. For a given momentum and mass hypothesis, a predicted time-of-flight t_{track} can be calculated. The momentum is determined by the tracking system, and the measured time-of-flight t_{tof} is provided by either the CTOF or the CND. The chosen mass hypothesis is the one minimizing the difference $t_{tof} - t_{track}$ (more details are given in section 4.2.1).

3.3.4 CLAS12 Forward Detector (FD)

The Forward Detector (FD) of CLAS12 is located downstream of the target. It aims at detecting particles with polar angles between 5° and 35° . It is divided into six

sectors, each equipped with the same set of sub-systems.

As for the Central Detector, a tracking system and time-of-flight detectors allow for the reconstruction of particle momenta and their identification. The forward tracking is achieved using three consecutive regions of Drift Chambers (DC), each divided into six sectors. The Forward Time Of Flight (FTOF) detector is located downstream of the DCs and is used to measure the time of flight of charged and neutral particles emitted in the FD. It is also divided into six sectors, each composed of three panels of double-sided readout plastic scintillator paddles.

The CLAS12 Electromagnetic Calorimeter (EC), located after the FTOF, consists of six independent calorimeters, one for each forward sector. The EC helps identify leptons and pions by measuring the deposited energy as they pass through the calorimeter.

There are two main Cherenkov detector systems in CLAS12: the High Threshold Cherenkov Counter (HTCC) and the Low Threshold Cherenkov Counter (LTCC). Cherenkov counters are usually filled with a large volume of gas (CO_2 for HTCC and C_4F_6 for LTCC). A particle crossing the gas volume at a speed greater than the speed of light in the medium emits a cone of light. This phenomenon, known as the Cherenkov effect, allows particle identification since light is emitted only if the particle momentum exceeds a threshold p_{th} that depends on the particle mass (see section 4.2.2 for more details).

4 Measurement of the cross section of the photo-production of ϕ with CLAS12

4.1 ϕ quasi-real photoproduction

In the CLAS12 experiment, electrons accelerated by the *CEBAF* accelerator interact with protons in the liquid hydrogen target via an intermediate photon. In the case of the photoproduction of a phi meson $ep \rightarrow (e')\gamma p \rightarrow (e')\phi p'$, we are only interested in events where the beam electron emitted a real photon. In practice, events where photon have a small virtuality will be selected (quasi-real photoproduction). The flux of real photons originating from the electron beam can be modeled using the Equivalent Photon Approximation (EPA) and a modeling of the Bremsstrahlung effect (see section 4.8).

Figure 6 shows a diagrammatic representation of the production of a ϕ meson off a proton. From the initial and final four-vectors of the target proton P and P' , we can calculate the Mandelstam variable t :

$$t = (P - P')^2. \quad (9)$$

The variable Q^2 is the square of the four-momentum transfer of the scattered electron and also represents the virtuality of the photon. It is defined as:

$$Q^2 = -q^2 = (k - k')^2. \quad (10)$$

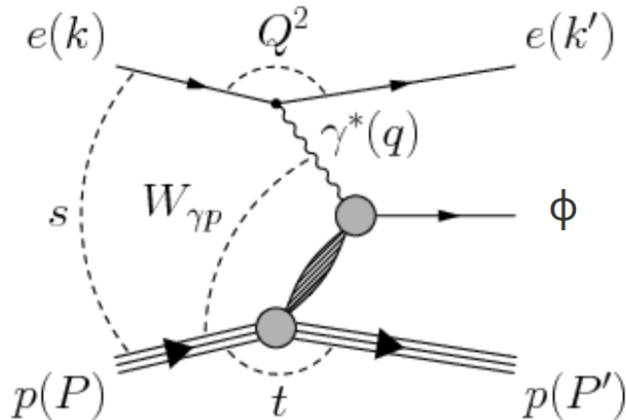


Figure 6: Diagram of ϕ quasi-real photoproduction on the proton. A virtual photon γ^* with four-momentum q mediates the interaction between an electron e with four-momentum k and a proton p with four-momentum P . t represents the square of the four-momentum transfer to the recoil proton p with momentum P' . Q^2 represents the squared four-momentum transfer to the scattered electron e with momentum k' and is equal to the virtuality of the photon γ^* . Adapted from [10].

To calculate the virtuality of the photon, we use the reconstructed electron angle θ and the following formula for Q^2 :

$$Q^2 = 2E_i E_f (1 - \cos \theta), \quad (11)$$

where E_i and E_f are the initial and final energies of the incident electron.

The photon energy is calculated by:

$$E_\gamma = E_{p'} - M_p + E_{e^-} + E_{e^+}, \quad (12)$$

where M_p is the proton mass, $E_{p'}$ the energy of the scattered proton, and E_{e^-} and E_{e^+} the energies of the electron and positron from the ϕ .

For each detected event containing an electron and a positron, the invariant mass is calculated as:

$$m_{inv}^2 = (p_{e^-} + p_{e^+})^2, \quad (13)$$

where p_{e^-} and p_{e^+} are the four-momenta of the electron and positron. If the electron and positron originate from the decay of a ϕ meson, the invariant mass m_{inv} is equal to the mass of the ϕ (1.019 GeV).

A final important parameter to introduce is the missing mass, noted MM , defined by:

$$MM^2 = (P + k - \sum_k p_k)^2. \quad (14)$$

P and k represent respectively the four-vectors of the proton and beam electron in the initial state, and $\sum_k p_k$ is the sum of the four-vectors of the detected particles in the final state. A missing mass close to zero ensures that, apart from the scattered electron, all final-state particles have been detected and the process is indeed an exclusive ϕ production [11].

4.2 Particle identification

The objective of this section is to present how, from the response of the detectors presented in chapter 3, a list of detected particles can be built along with their momenta and vertex positions [12]. The procedure to identify proton will be described in section 4.2.1 and the one for electron in section 4.2.2

4.2.1 Proton identification

As discussed in section 3.3.1, the momentum of detected particles is calculated using the curvature radius of the trajectory of the particle R and the magnetic field B via equation 8. The momentum alone is not sufficient to identify the type of particle. However, by measuring the time of flight and correlating it with the momentum

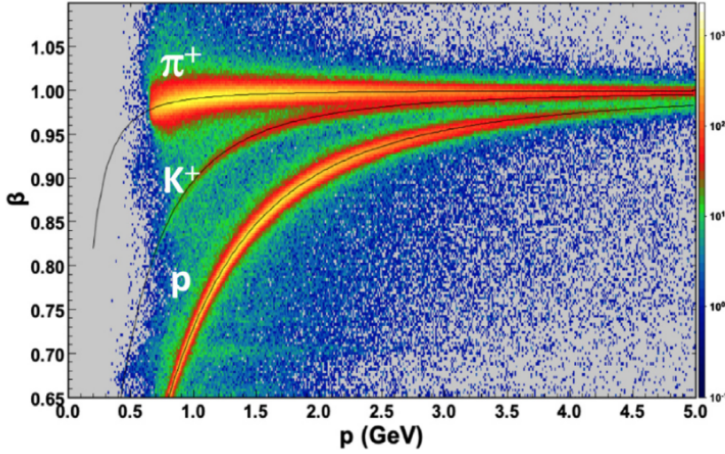


Figure 7: Velocity β versus p momentum, where the velocity is measured for all positively charged particle which have been also detected in the FTOF. Three distinct bands can be identified for positively charged pions (π^+), positively charged kaons (K^+) and protons (p).

p , the mass of the detected particle can be estimated and thus the particle identified.

The time of flight t_{tof} is determined with :

$$t_{tof} = t_{det} - t_s, \quad (15)$$

where t_{det} is the time associated with the Time Of Flight (TOF) detectors. There are two TOF detectors in CLAS12: FTOF in the FD and CTOF in the CD (see chapter 3). t_s corresponds to the initial interaction time between the beam electron and the proton. It is determined using the time measured by a trigger particle in the FTOF. In practice, the fastest particle of the event is used, such as an electron, and is assumed to travel at the speed of light. The event start time t_s is obtained by correcting the travel time t of the trigger particle by the path length (the distance between the vertex and the hit of the particle in the FTOF) dividing by c . This distance is estimated from the track left in the DCs. We then have the formula:

$$t_s = t - \frac{L}{c}, \quad (16)$$

with t the time of the trigger particle in the FTOF and L the path length.

The expected TOF from tracking t_{track} is given by:

$$t_{track} = \frac{L \sqrt{p^2 + m^2 c^2}}{pc}, \quad (17)$$

where m is the mass of the particle and p its momentum. The mass hypothesis that minimizes $t_{tof} - t_{track}$ is assigned to the particle. Figure 7 shows the relationship between the velocity β (obtained with t_{tof}) and momentum in the FD.

4.2.2 Electron and positron identification

Given the low mass of electrons and positrons, they are detected in the Forward Detector (FD). Their momentum is measured in the Drift Chambers (DCs) and their energy in the Electromagnetic Calorimeter (EC). To identify a particle as an electron or positron, it's not possible to use the same identification method used for protons in the Central Detector (CD). Indeed, the resolution of the Forward Time Of Flight (FTOF) is too low to distinguish leptons from pions. As a result, electrons and positrons are identified using the Sampling Fraction (SF) of the EC and the number of photoelectrons detected in the High Threshold Cherenkov Counter (HTTC). The SF is defined as:

$$SF = \frac{E_{dep}}{P}, \quad (18)$$

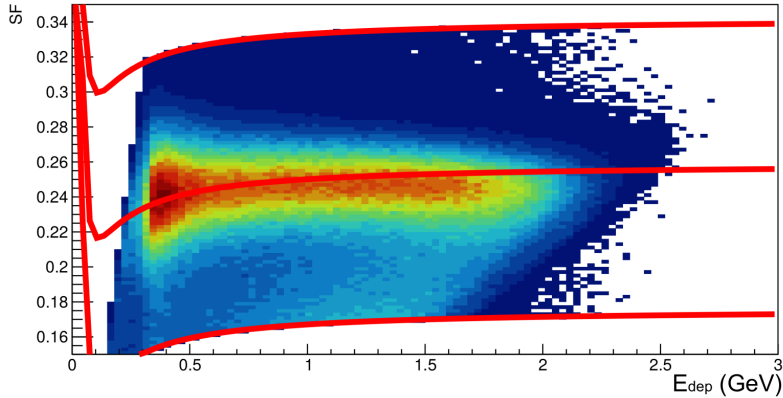


Figure 8: SF versus E_{dep} for electrons in the EC, from data. The three red curves represent the parametrized SF_M extracted from simulations, and its 5σ limits.

where E_{dep} is the total energy deposited in the EC and P the momentum measured in the DCs. Once these two quantities are measured, it is possible to calculate the SF ratio, which significantly depends on the particle type. Typically, as shown in Figure 8, the SF is approximately 0.25 for an electron or a positron. The SF is much lower (about 0.02) for pions, since they deposit much less energy in the EC than electrons or positrons for the same momentum. Pions deposit less energy because, at JLab energies (a few GeVs), they are minimum ionizing particles. The first identification criterion is therefore to obtain a SF close to a parametrized SF_M (obtained by simulation) within a 5σ limit.

The second identification criterion relies on the number of photoelectrons detected in the HTTC. There is a threshold momentum p_{th} for a particle of mass m above which it begins to emit Cherenkov light in a medium of refractive index n . It is defined as:

$$p_{th} = \frac{mc}{\sqrt{n^2 - 1}}, \quad (19)$$

where m is the particle's mass and n the refractive index of the medium. Given the low mass of electrons and positrons, their p_{th} is very small, and they always emit photon in the HTTC. Then the light is collected and a photo-multipliers (PMT) will collect this light and turn it into electric signal, which can be measured. This signal is quantified in terms of photo-electrons. On the other hand, due to their higher mass, the momentum threshold for pions is 4.9 GeV. Thus, if photoelectrons are detected in the HTTC (at least 2) for a particle with momentum below 4.9 GeV, it is identified as a lepton, and not as a pion. Above 4.9 GeV, both pions and leptons emit Cherenkov light, and this criterion can no longer be used.

To identify particles with momentum above 4.9 GeV, only the EC criterion is available. The EC-based selection can be improved by analyzing the spatial distribution of the energy deposits, since electrons and positrons tend to produce electromagnetic showers, unlike pions. This method has been developed in [13] and [14] and is also used in this analysis.

4.3 Events selection

This section explains how the events are selected before performing the extraction of the ϕ yield. The data acquired between 2018 and 2019 by CLAS12 (RG-A with LH_2 target) is stored in ROOT files containing the four-momenta of the detected particles. The data could be acquired in outbending or inbending mode during this period. The difference between inbending and outbending lies in the orientation of the torus magnetic field. To experimentally tag the photoproduction of a ϕ , we detect the decay products along with the recoil proton. In this analysis, we focus on the leptonic decay channel $\phi \rightarrow e^+e^-$. Events containing a proton, an electron, and a positron are therefore considered. The following cut is applied to the entire set of events to ensure that an exclusive reaction was detected :

$$|MM|^2 < 0.3 \text{ GeV}^2, \quad (20)$$

where $|MM|$ is the missing mass defined by 14. A second cut is applied to the entire set of events to ensure it is quasi-real photoproduction of ϕ :

$$Q^2 < 0.3 \text{ GeV}^2, \quad (21)$$

where Q^2 , defined in the equation 10, is the virtuality of the incident photon. Figure 9 shows the invariant mass spectrum of the events selected for this analysis.

In Figure 9 no cut is applied on the photon energy in order to obtain an estimate of the total number of ϕ . Peaks can be seen, corresponding to the exclusive photo-production of π^0 (134 MeV), ρ (776 MeV), ω (782 MeV), and ϕ (1019 MeV). It is considered an invariant mass window (between 0.95 and 1.05 GeV) associated to a ϕ meson.

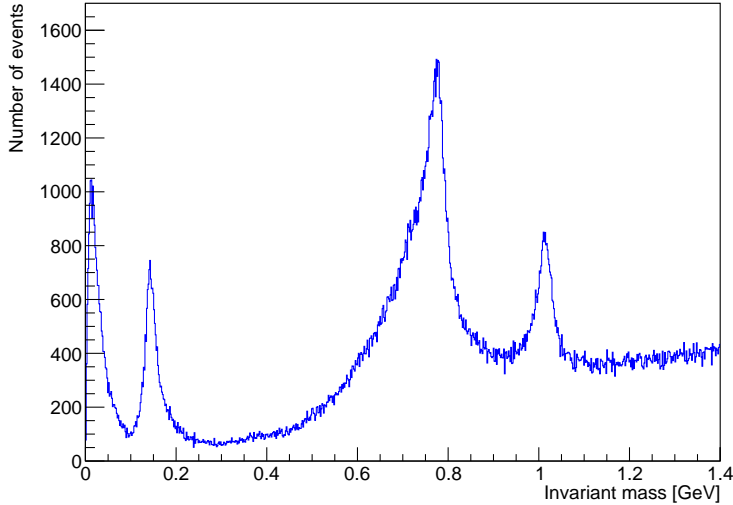


Figure 9: Histogram of invariant mass in e^+e^- canal.

4.4 Experimental cross section

The total cross section $\sigma(E_\gamma)$ and the differential cross section $\frac{d\sigma(E_\gamma)}{dt}$ represent the probability of producing a ϕ meson when an electron from the beam interacts with a proton in the liquid hydrogen target via a quasi-real photon. The total cross section is calculated per photon energy bin, while the differential cross section is calculated per bin in t within a fixed photon energy range. These cross sections are obtained using the following two formulas:

$$\sigma(E_\gamma) = \frac{N_\phi(E_\gamma)}{L \times F(E_\gamma) \times A \times E \times Br}, \quad (22)$$

$$\frac{d\sigma(E_\gamma)}{dt} = \frac{N_\phi(E_\gamma)}{L \times F(E_\gamma) \times A \times E \times Br \times \Delta t}. \quad (23)$$

N_ϕ represents the number of ϕ mesons detected per photon energy bin. It is obtained by fitting the invariant mass distribution around the ϕ meson mass and integrating the signal. The term $A \times E$ represents the acceptance-efficiency of CLAS12 for the reaction. This term accounts for how the detector's geometry and efficiency affect the number of detected ϕ mesons. Br represents the branching ratio in the e^+e^- decay channel, which is equal to 2.954×10^{-4} . This term accounts for the fact that we calculate the number of ϕ mesons from only one decay channel, even though there are several others. Finally, the product $L \times F(E_\gamma)$ gives the quasi-real photoproduction luminosity. L includes information about the target, such as its density and length, as well as about the electron beam, such as the accumulated charge. $F(E_\gamma)$ is used to estimate the number of quasi-real photons emitted within a given energy interval (i.e., the considered E_γ bin) per electron.

4.5 Extraction of the ϕ meson yield

This section explains how to extract the ϕ yield from the selected events (see section 4.3). For each event, one can compute the invariant mass from the four-momenta of the electron and positron using the relation 13. If the electron and positron are associated with the decay of a ϕ , the invariant mass will be close to the mass of the ϕ (1.019 GeV). The number of ϕ is therefore equal to the integral of the invariant mass peak located around 1.019 GeV.

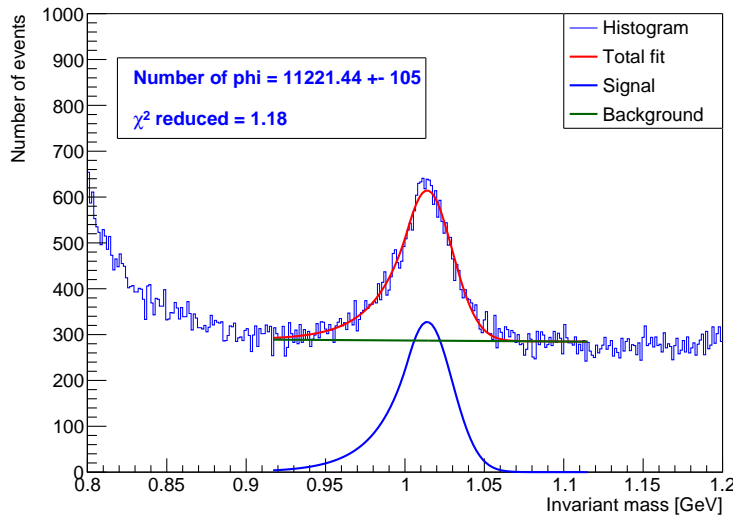


Figure 10: Fit of the invariant mass spectrum in a region of the ϕ . The total fit function is represented in red, the background function in green, and the signal in blue.

Figure 10 shows a fit of the ϕ peak using a parametric function of the form $ax + b + f(x)$, where the linear function models the background and the function $f(x)$ is a Crystal Ball function which models the signal.

The Crystal Ball function is defined as:

$$f(x; \alpha, n, \bar{x}, \sigma) = \begin{cases} A \left(\frac{n}{|\alpha|} \right)^n e^{-\frac{|\alpha|^2}{2}} \left(\frac{n}{|\alpha|} - |\alpha| - \frac{x - \bar{x}}{\sigma} \right)^{-n} & \text{if } \frac{x - \bar{x}}{\sigma} \leq -|\alpha| \\ Ae^{-\frac{(x - \bar{x})^2}{2\sigma^2}} & \text{if } \frac{x - \bar{x}}{\sigma} > -|\alpha| \end{cases} \quad (24)$$

where \bar{x} is the mean, σ is the standard deviation of the Gaussian, α determines the position of the break, n controls the tail shape, and A is a normalization factor.

The fit in figure 10 allow to extract the background and signal parameters separately. The integral of this signal allows us to obtain the number of detected ϕ .

251 ϕ are found in the combination of all datasets.

Since the uncertainty on the cross section is approximately $\frac{1}{\sqrt{N_\phi}}$, where N_{phi} is the number of ϕ , it is important to have the same number of ϕ per photon energy bin in order to have approximately the same uncertainty on the cross section per bin of photon energy. The photon energy range ([2 - 12 GeV]) is then split into bins of variable size. The minimum is set at 2 GeV because the photon must have at least 1.57 GeV to produce a ϕ , and no events are reconstructed below 2 GeV. The maximum photon energy is limited by the beam electron energy, which is 10.6 GeV.

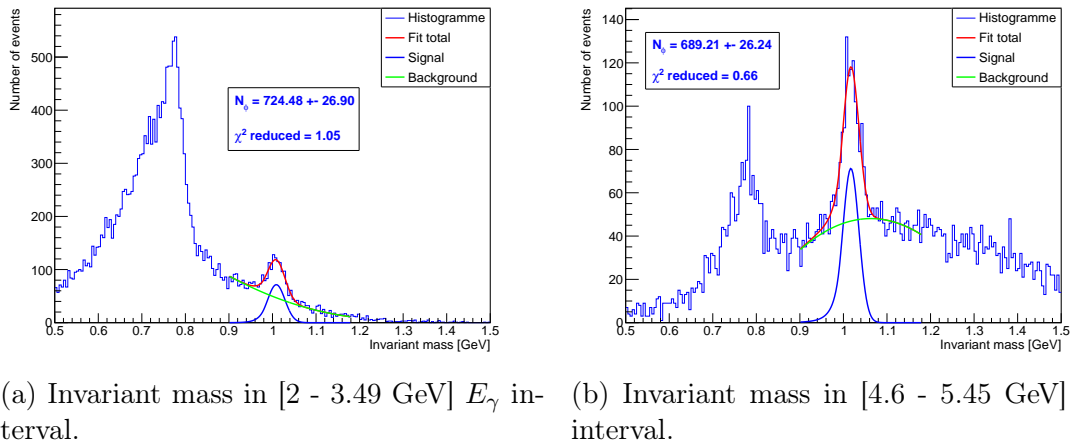


Figure 11: Example of a fit to extract the number of ϕ in different photon energy interval.

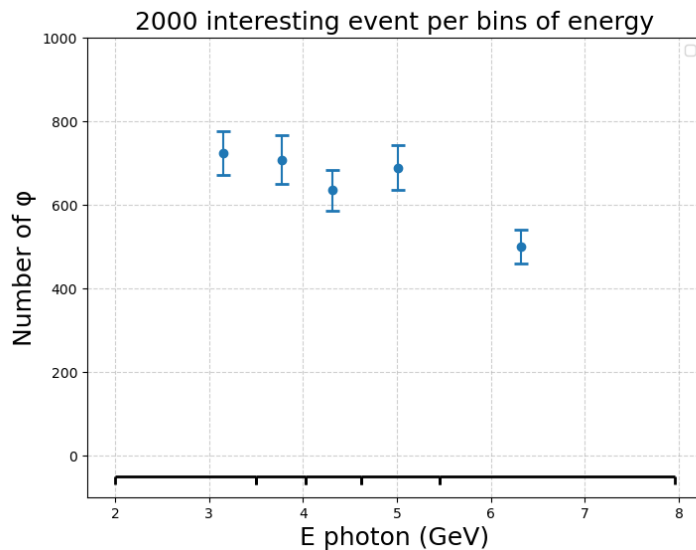


Figure 12: N_ϕ for each bin in photon energy.

From an algorithmic perspective, the bin sizes are adjusted so that they all contain the same number of events near the ϕ mass between 0.95 and 1.05 GeV, while applying previous cuts on Q^2 and missing mass. These events are not necessarily associated with a ϕ and may come from background, but this provides a first approximation of the number of ϕ . Once the variable-sized bins are established, we perform the fit of the peak and find the exact number of ϕ per photon energy bin (some examples are given in figures 11a and 11b). Figure 12 shows the number of ϕ associated with each photon energy bin. One can see that each bin contains approximately the same number of ϕ .

4.6 Acceptance estimation

The detector geometry, as well as its efficiency, does not allow for the detection of all produced ϕ mesons. Therefore, the cross section must be corrected with the probability of detecting an event in the detector, taking into account its limited angular coverage and efficiency. To obtain the acceptance of CLAS12, the ratio between the number of reconstructed events by the detector and the number of events generated is determined. A number N_{gen} of ϕ photoproduction events are generated and sent through GEMC, the CLAS12 simulation software [15].

4.6.1 Generator of ϕ events

This section presents the event generator for the photoproduction of the ϕ meson which has been developed during this internship. The ‘TGenPhaseSpace’ class from ROOT is used to generate decay events in the context of high-energy physics [16]. It allows the simulation of the decay of a parent particle into several daughter particles while respecting conservation laws of energy and momentum. It generates events according to a uniform distribution in phase space. Four-momenta are represented by the ‘TLorentzVector’ class, whose components are (p_x, p_y, p_z, E) . The following four-momentum is associated with the proton target in the laboratory frame:

$$P = (0, 0, 0, M_p), \quad (25)$$

where M_p is the mass of the proton (0.938 GeV). The four-momentum of the incident photon is defined by:

$$\gamma = (0, 0, E_\gamma, E_\gamma), \quad (26)$$

where E_γ is the energy of the incident photon. For each event, E_γ is determined by a uniform random draw between $E_{min} = 1.58$ GeV and $E_{max} = 10.6$ GeV. For each event, the ‘TGenPhaseSpace’ class is used to generate a decay of the four-momentum $W = P + \gamma$ into two particles whose masses are specified. Here, the two daughter particles are the recoil proton P' and the ϕ meson. A second decay of the ϕ meson into an electron-positron pair is then performed using the same method. It is the four-momenta of these electron-positron pairs that are then sent to the CLAS12 GEMC simulation.

Not all generated events are equally probable, so they must be assigned weights. To take into account the probability that the photon has an energy E_γ , the event must be weighted by the factor w_γ , which represents the probability density associated with the emission of a photon of energy E_γ by an electron from the beam (this probability density is detailed in 4.8). A weight $w_{\gamma 2} = E_{max} - E_{min}$ is also added to account for the initial sampling range. One must also add a weight $w_t = |t_{min} - t_{max}|$ where t_{min} and t_{max} represent, respectively, the minimal and maximal kinematically allowed values of t (equation 9), since ‘TGenPhaseSpace’ only generates events within the kinematically allowed phase space. The branching ratio for decay into an e^+e^- pair is also taken into account with $w_{BR} = 2.9 \times 10^{-4}$.

A model developped for J/ψ production in [17] was adapted to the ϕ case and used to model the t dependance of the cross section in this generator. Finally, the t -dependence of the ϕ production process is taken into account with a weight w_{dcs} . In the end, each event is weighted by a total weight w defined as:

$$w = w_\gamma \cdot w_{\gamma 2} \cdot w_t \cdot w_{BR} \cdot w_{dcs}. \quad (27)$$

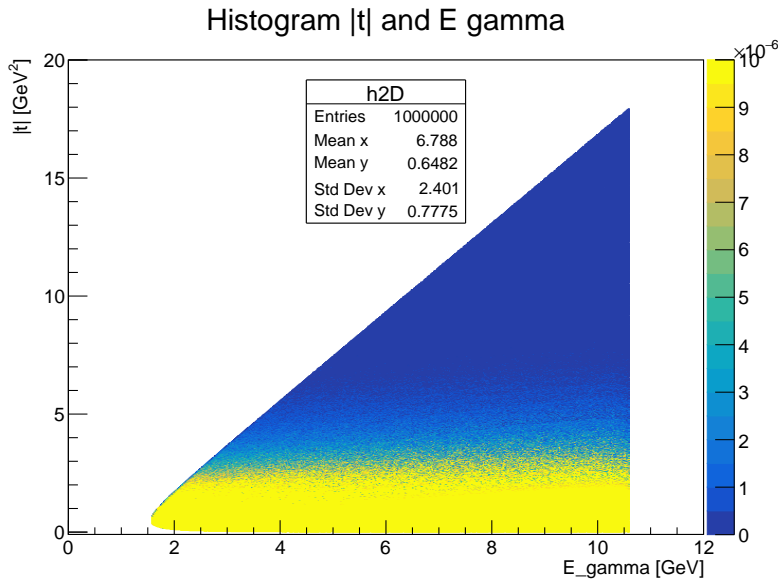


Figure 13: 2D histogram representing $|t|$ vs E_γ .

Figure 13 shows a 2D histogram of $|t|$ versus E_γ for generated events. Since the differential cross section for ϕ photoproduction decreases as a function of $|t|$, significantly fewer events are observed at large values of $|t|$.

Figures 14a and 14b show 2D histograms of the momentum p and angle θ for the generated electron and proton. The electron is mostly generated with a small angle θ and will be well detected in the FD. The proton is generated with low momentum and a large angle, and will be detected in the CD.

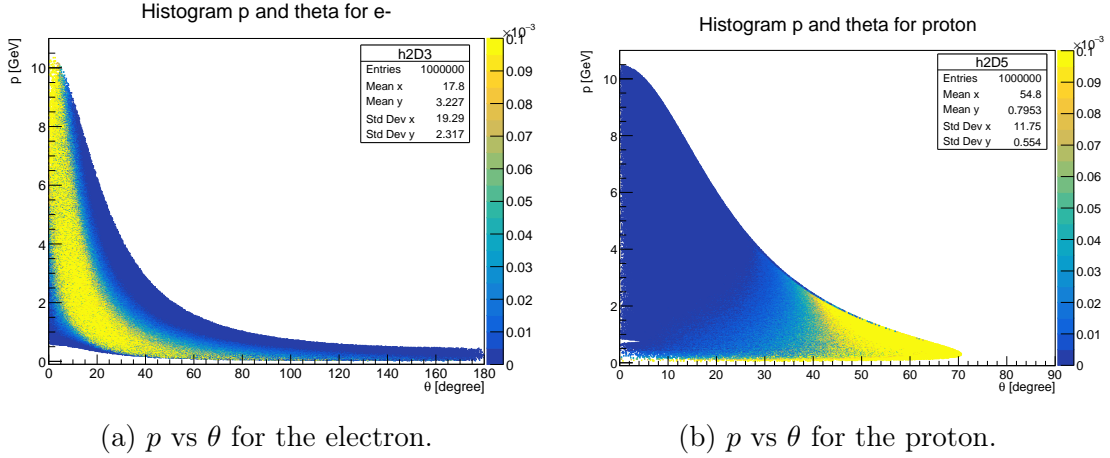


Figure 14: 2D histogram of p vs θ for the electron and the proton

4.6.2 Acceptance estimation

The GEMC simulation yields a ROOT file as output, similar to the real data. In the histogram of invariant mass of the reconstructed electron-positron pairs, a single peak is observed at the ϕ mass.

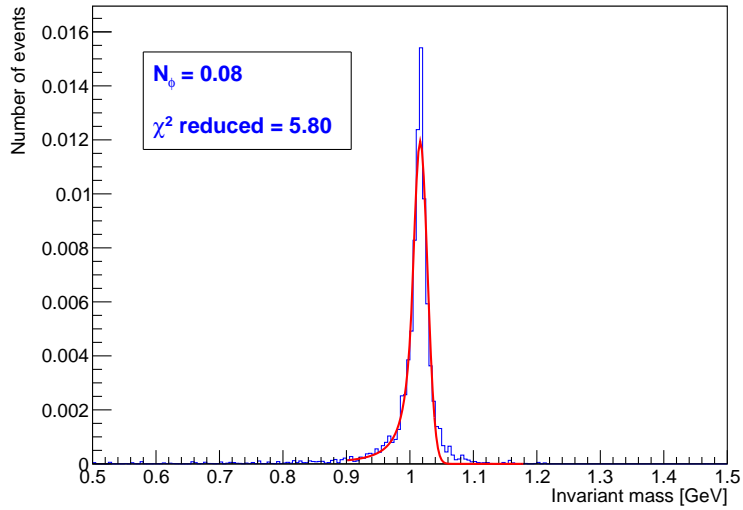


Figure 15: Example of a fit of the invariant mass peak from the simulated data.

As shown in figure 15 by performing a Crystal Ball fit over the same invariant mass range as for the real data, the number N_{rec} of reconstructed ϕ mesons is estimated. The ratio N_{rec}/N_{gen} allows to estimate the acceptance per photon energy bin as seen in figure 16.

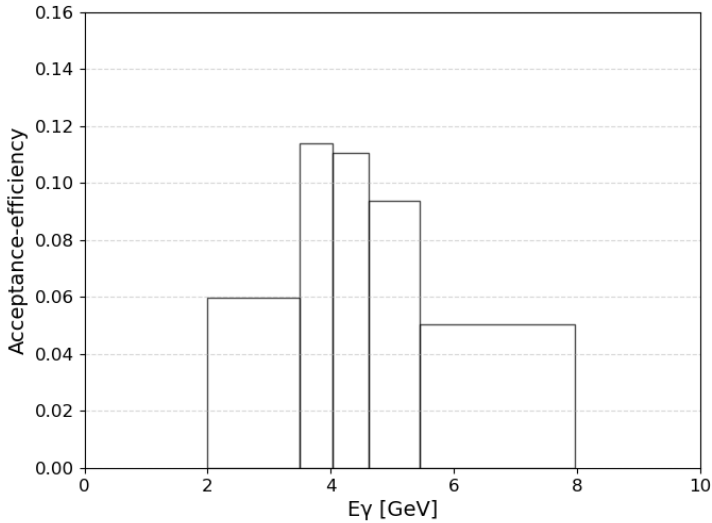


Figure 16: Acceptance-efficiency per photon energy γ bin.

4.7 Luminosity of the RGA dataset

The integrated luminosity measures the number of potential collisions per unit time and surface. It is defined as:

$$L = \rho_{proton} \cdot l \cdot N_{e^-}, \quad (28)$$

where ρ_{proton} is the proton density in the target, l is the target length, and N_{e^-} is the number of electrons sent onto the target. We can rewrite the integrated luminosity as:

$$L = \frac{2 \times N_a \times \rho_{H_2} \times l}{e \times M} * Q, \quad (29)$$

where N_a ($6.02214 * 10^{23}$) is Avogadro's number, ρ_{H_2} (0.0709 g/cm^3) is the mass density of liquid hydrogen, M (2.016 g/mol) is the molar mass of di-hydrogen, e ($1.602176634 * 10^{-19} \text{ C}$) is the electron charge, and Q (114.112 mC) is the accumulated charge during the experiment. The factor of 2 comes from the fact that there are two protons per di-hydrogen molecule. For the tree data set, the integrated luminosity is $150843.80 \text{ pb}^{-1}$.

4.8 Photon flux calculation

As the objective of this analysis is to measure the photoproduction cross section and not the electroproduction one, normalization must be done not by the number of electrons sent on the target but by the number of quasi-real photons which have been emitted. It is therefore necessary to consider the number of quasi-real photons emitted per electron in a given energy interval. Multiplying the integrated luminosity by this flux allows one to convert the term N_{e^-} into N_{gamma} in equation 29

corresponding to the number of photons sent onto the target for a given energy bin.

To compute this flux, it is necessary to integrate the flux density over a energy bin of the photon. According to ref [18] and [19], the flux density $F(x)$ can be estimated as:

$$F(x) = F_{epa} + F_{brem}, \quad (30)$$

$$F_{epa} = \frac{1}{E_b} \cdot \frac{\alpha}{\pi x} \left(\left(1 - x + \frac{x^2}{2} \right) \ln \left(\frac{Q^2_{\max}}{Q^2_{\min}} \right) - (1 - x) \right), \quad (31)$$

with $x = \frac{E_g}{E_b}$, and

$$F_{brem} = \left(\frac{0.5 \cdot d}{X_0} \right) \cdot \left(\frac{1}{E_g} \right) \cdot \left(\frac{4}{3} - \frac{4}{3} \cdot \frac{E_g}{E_b} + \frac{E_g^2}{E_b^2} \right). \quad (32)$$

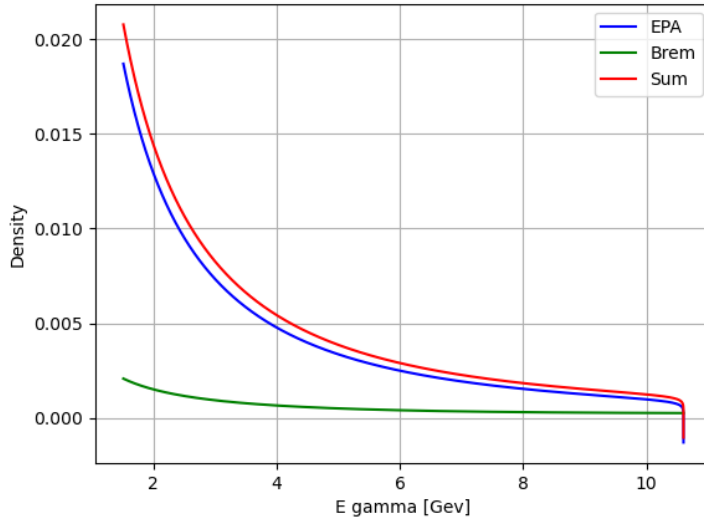


Figure 17: Photon flux density as a function of photon energy. In blue the contribution from quasi-real photons emitted at the time of interaction between the electron and proton and in green the photon flux density associated with Bremsstrahlung affect. The curve in red is the sum of these two contributions.

The F_{epa} term models the contribution from quasi-real photons emitted at the time of interaction between the electron and proton. We set the virtuality limit at $Q^2 = 0.02$ GeV as this is the maximum virtuality for which the electron is not detected in the forward tagger of CLAS12. The F_{brem} term models the flux density of real photons emitted via Bremsstrahlung as the electron passes through the target. Figure 17 shows both contributions and their sum as a function of E_γ .

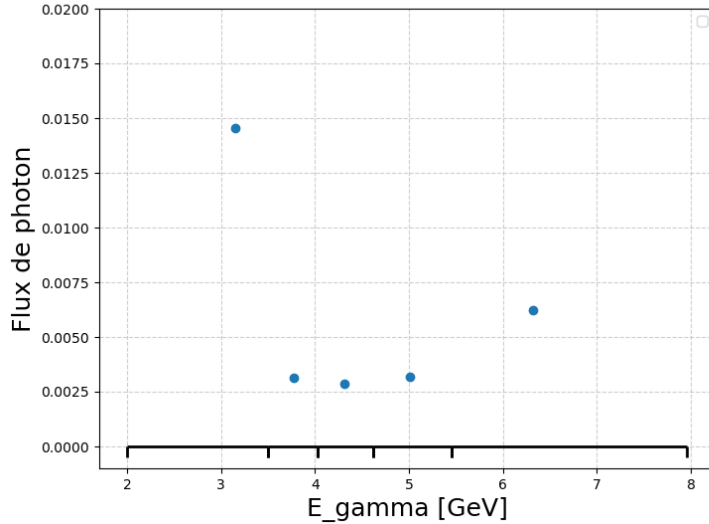


Figure 18: Integrated photon flux per bin of photon energy.

After integration, we obtain the photon flux $F(E_\gamma)$ per bin of photon energy as seen in figure 18.

4.9 Results on cross section and differential cross section

The photoproduction cross section of the ϕ meson is thus determined using the previous results and the formula in section 4.4. In Figure 19, the results of this analysis are compared with a previous analysis using CLAS12 data [14].

The differential cross section has also been calculated. In this case, a photon energy bin is fixed and the differential cross section is calculated for several bins in $|t|$ using the formula presented in 4.4. Figure 20 shows the results obtained in the photon energy range [3.6 - 4.3 GeV]. The cross section is falling with large t , which is the expected behaviour.

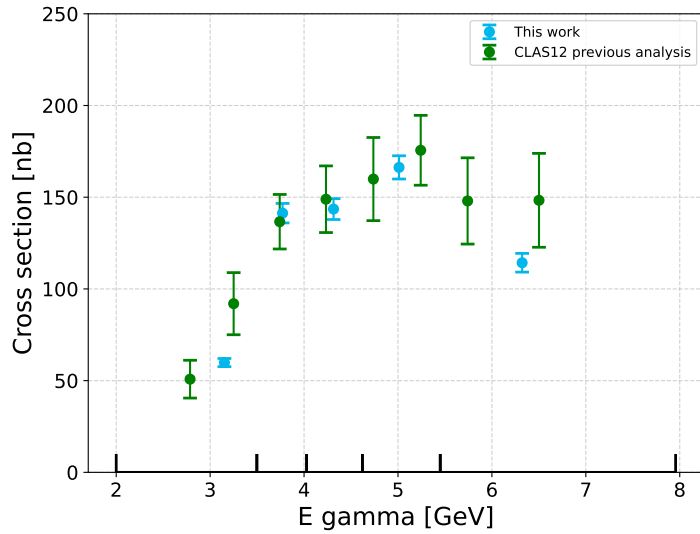


Figure 19: Cross section of the photoproduction of ϕ . In blue this work and in green a previous analysis of ϕ photoproduction with CLAS12.

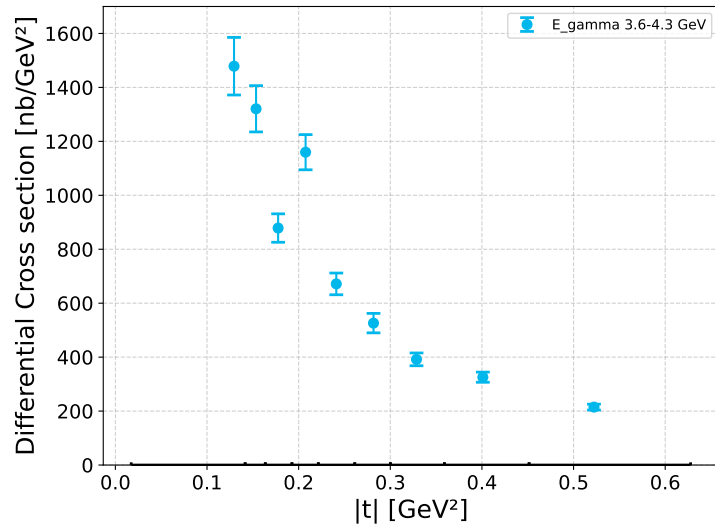


Figure 20: Differential cross section in the range [3.6 - 4.3 GeV] of E_{γ} .

5 Conclusion and outlook

This research internship was part of a broader effort to study the internal structure of the proton through the analysis of the exclusive photoproduction of the ϕ meson using the CLAS12 detector. Specifically, the objective was to extract the total and differential cross sections of the process $\gamma p \rightarrow \phi p$ in the leptonic decay channel $\phi \rightarrow e^+e^-$.

After an introduction to the theoretical framework of Generalized Parton Distributions (GPDs) and the physical motivations related to gluon dynamics, a substantial amount of work was carried out on the analysis of experimental data. This required a careful selection of exclusive events as well as the estimation of the detector acceptance using a Monte Carlo event generator.

The cross section was determined by accounting for the beam luminosity, the quasi-real photon flux, and the acceptance factor obtained from simulations. The results are in agreement with previous analyses. The next step will involve interpreting these results to gain a deeper understanding of the gluonic structure of the proton.

It also opens up interesting perspectives, such as improving statistical precision, exploring other decay channels, or using these measurements to place direct constraints on theoretical GPD models.

References

- [1] Ian Hinchliffe and Aneesh V. Manohar. The qcd coupling constant. *Annual Review of Nuclear and Particle Science*, 50, 04 2000.
- [2] A. D. Martin, W. J. Stirling, R. S. Thorne, and G. Watt. Parton distributions for the lhc. *The European Physical Journal C*, 63(2):189–285, Sep 2009.
- [3] A. V. Radyushkin. Nonforward parton distributions. *Phys. Rev. D*, 56:5524–5557, Nov 1997.
- [4] D. Müller, D. Robaschik, B. Geyer, F.-M. Dittes, and J. Horejesi. Wave functions, evolution equations and evolution kernels from light-ray operators of qcd. *Fortschritte der Physik/Progress of Physics*, 42(2):101–141, 1994.
- [5] Nicole d’Hose, Silvia Niccolai, and Armine Rostomyan. Experimental overview of deeply virtual compton scattering. *The European Physical Journal A*, 52(6):151, Jun 2016.
- [6] Wang, R., Kou, W., Xie, Y.-P., Chen, X. (2021). Extraction of the proton mass radius from the vector meson photoproductions near thresholds. *Physical Review D*, 103(9).
- [7] Reza Kazimi. Simultaneous Four-hall Operation for 12 GeV CEBAF. In 4th International Particle Accelerator Conference, page THPFI091, 2013.
- [8] V.D. Burkert et al. The clas12 spectrometer at jefferson laboratory. *Nuclear Instruments and Methods in Physics Research Section A: Accelerators Spectrometers, Detectors and Associated Equipment*, 959:163419, 2020.
- [9] N. Baltzell et al. The clas12 beamline and its performance. *Nuclear Instruments and Methods in Physics Research Section A: Accelerators, Spectrometers, Detectors and Associated Equipment*, 959:163421, 2020.
- [10] K. Tu (STAR Collaboration), J/ψ photoproduction off deuteron in d+Au UPC at STAR (2020).
- [11] D.J.Griffiths, *Introduction to elementary particles* Wiley, 2nd rev. version, 2008.
- [12] V.Ziegler et al. The clas12 software framework and events reconstruction. *Nuclear Instruments and Methods in Physics Research Section A: Accelerators, Spectrometers, Detectors and Associated Equipment*, 959:163472, 2020.
- [13] Pierre Chatagnon. Nucleon structure studies with CLAS12 at Jefferson Lab : timelike Compton scattering and the central neutron detector. *High Energy Physics - Experiment [hep-ex]*. Université Paris-Saclay, 2020. English. NNT : 2020UPASP039. tel-03041549
- [14] Tyson, Richard (2023) J/ψ near-threshold photoproduction off the proton and neutron with CLAS12. PhD thesis.

- [15] M. Ungaro et al. The clas12 geant4 simulation. Nuclear Instruments and Methods in Physics Research Section A: Accelerators, Spectrometers, Detectors and Associated Equipment, 959:163422, 2020.
- [16] <https://root.cern.ch/doc/master/classTGenPhaseSpace.html>
- [17] PHYSICAL REVIEW D 106, 086004 (2022)
- [18] C.J. Brown, D.H. Lyth, Assessment of the equivalent photon approximation for the process $ee \rightarrow ee\pi + \pi-$, Nucl. Phys. B, 53 2 (1973).
- [19] T.H. Burnett, The diagonal equivalent photon density matrix: An exact extension of the equivalent photon approximation, Nucl. Phys. B, 114, 1 (1976).